In Vivo Skin Penetration of Quantum Dot Nanoparticles in the Murine Model: the Effect of UVR

Luke Mortensen[1], **Gunter Oberdörster**[2], **Alice P. Pentland**[3], and **Lisa A. DeLouise**[1,3,*]

[1]Department of Biomedical Engineering, University of Rochester, Rochester NY, 14642 United States of America

[2]Department of Environmental Medicine, University of Rochester, Rochester NY, 14642 United States of America

[3]Department of Dermatology, University of Rochester, Rochester NY, 14642 United States of America

Abstract

Ultraviolet radiation (UVR) has widespread effects on the biology and integrity of the skin barrier. Research on the mechanisms that drive these changes, as well as their effect on skin barrier function has been ongoing since the 1980s. However, no studies have examined the impact of UVR on nanoparticle skin penetration. Nanoparticles (NP) are commonly used in sunscreens and other cosmetics, and since consumer use of sunscreen is often applied to sun damaged skin, the effect of UVR on NP skin penetration is a concern due to potential toxicity. In this study we investigate nanoparticle skin penetration by employing an *in vivo* semiconductor quantum dot nanoparticle (QD) model system. This model system improves NP imaging capabilities and provides additional primary interest due to widespread and expanding use of QD in research applications and manufacturing. In our experiments, carboxylated QD were applied to the skin of SKH-1 mice in a glycerol vehicle with and without UVR exposure. The skin collection and penetration patterns were evaluated 8 and 24 hours after QD application using tissue histology, confocal microscopy, and transmission electron microscopy (TEM) and EDAX analysis. Low levels of penetration were seen in both the non-UVR exposed mice and the UVR exposed mice. Qualitatively higher levels of penetration were observable in the UVR exposed mice. These results are the first for *in vivo* QD skin penetration, and provide important insight into the ability of QD to penetrate intact and UVR compromised skin barrier. Our findings raise concern that NP of similar size and surface chemistry, such as metal oxide NP found in sunscreens, may also penetrate UV damaged skin.

Introduction

One of the fastest growing scientific fields is that of nanoscale discovery and application. This growth has translated into an explosion in the amount of nanoparticles (NP) that are used every day in a wide variety of scientific disciplines and consumer products. NP are used in applications ranging from targeted fluorescent labels in the life sciences[1], ultraviolet

*lisa_delouise@urmc.rochester.edu; Tel: 585-275-1810.

radiation (UVR) protective cosmetics[2], and bacterial inhibitors[3] in food storage containers to wound care products and baby pacifiers. Concurrent with this growth, however, are increasing environmental and human health concerns[4,5]. Of particular concern are UVR protective cosmetics and sunscreens. These consumer products often contain significant amounts (~5-10% by weight) of ZnO and TiO_2 NP (<20 nm dia)[6] and they are marketed to diverse consumer groups (children and adults) for use on a daily basis. SPF (sun protection factor) containing products are often applied on a repeated basis to skin that has suffered sun exposure sufficient enough to have initiated biological UVR-induced skin repair processes. As described below, these processes are known to weaken inside-out skin barrier function as measured by transepidermal water loss, which is believed to result from a disorganization of the intercellular lipid lamallae[7]. Therefore, it is important to ascertain the potential effect of UVR exposure on the skin barrier function with respect to NP penetration.

The question of whether or not NP can penetrate the healthy stratum corneum skin barrier *in vivo* remains largely unanswered. Recent studies suggest that TiO_2 NP suspended in a cosmetic-type emulsion do not penetrate the stratum corneum when applied *ex vivo* to porcine skin[8] and *in vivo* to human skin[9,10,11]. The penetration of QD through skin was addressed by the Monteiro-Riviere research group employing an *ex vivo* porcine skin model. Their initial results found that with 8 hours and 24 hours of exposure to QD, porcine skin had a large amount of QD penetration throughout the epidermis and deep into the dermis in some cases[12]. In a more recent follow-up study, they reported contrasting results in that minimal penetration of QD through *ex vivo* porcine skin was found, with the bulk of the QD remaining in the stratum corneum[13]. Reasons for this discrepancy remain unclear, however, other researchers have examined the question of skin penetration employing different NP types (metals, polymers) using *ex vivo* skin models, and again contrasting results of both high and low levels of NP penetration are reported[14,15,16,17]. This suggests a lack of control over experimental variables and the need for standardization of experimental techniques if *ex vivo* skin models are to be useful. Moreover, these studies did not examine changes in skin permeability to NP penetration following exposure to activating UVR or when the stratum corneum is compromised by physical or chemical assault.

It is important to determine if NP can penetrate healthy and/or barrier compromised skin as potential toxicological consequences may result depending upon on whether NP are taken up by epidermal skin cells and/or translocated to secondary sites. *In vitro* studies have clearly established non-specific cell uptake[18], receptor mediated cell uptake[19], and cytotoxicity[20,21] of nanoparticles (metal oxides, quantum dots, carbon nanotubes, etc.) by many cell types including nerve cells[22], macrophage cells[23], dermal fibroblasts[24], keratinocytes[25] and others[22,26,27,28]. Early *in vitro* studies performed to assess the effects of QD on keratinocytes found non-specific cellular uptake that was independent of surface chemistry, a surface chemistry dependent inflammatory cytokine release, and dose dependent cytotoxicity[25]. It is a common finding that nanoparticle cytotoxicity results from the generation of reactive oxygen species (ROS)[28,29,30]. In the case of TiO_2 however, some studies fail to observe notable ROS generation[29,30,31]. This discrepancy likely relates to the dependence of ROS generation on TiO_2 crystal composition and to differences in experimental UVA light levels. UVA light dramatically increases ROS production from

both the rutile and anatase crystal forms of TiO_2 [28,29,30,32,33], however, anatase is significantly cytotoxic even in the absence of UVA[28,34]. This is a concern as the anatase form is common in the formulation of sunscreens[35].

Given the ability of NP to induce free radical cytotoxicity, the uncertainty regarding potential NP skin penetration within the *ex vivo* model, and the limited availability of *in vivo* data- especially in barrier compromised skin- examination of an *in vivo* and UVR exposure model is necessary. Herein we present our initial efforts to develop an *in vivo* model of nanoparticle skin penetration using the SKH-1 hairless mouse employing quantum dot (QD) nanoparticles. We selected to investigate QD, as they possess ideal characteristics for *in vivo* experimentation including broad excitability, narrow emission bandwidth, high fluorescence quantum yield, photostability, and ease of surface functionalization[36,37]. Moreover, QD are of a similar size to TiO_2 NP used in sunscreen applications (~1-30 nm), they intrinsically generate ROS species[20], and the carboxyl terminated QD have a similar negative oxide surface chemistry to TiO_2 and ZnO NP raw materials often used in sunscreen applications[8]. QD interaction with skin is also of primary interest, as the occurrence of QD in the life sciences and other technical applications is rising[4] and has consequently increased the risk of QD skin exposure to manufactures, researchers, and consumers.

We have selected the SKH-1 mouse for these studies as it is a well accepted model system for studying skin barrier function, UVR induced skin cancer, and other diseases due to its similar follicular density and dermal to epidermal differentiation[38,39]. In previous studies, the biological effect of UVR irradiation has been examined at a variety of acute and repeated doses[40,41]. Here, we are interested primarily in acute UVR exposure, as it is the most applicable to consumer use and has been shown to have a significant effect on skin barrier function at a range of doses[40]. To induce a level of UVR exposure that is similar to medium level sunburn in a human, a quantity of UVR (A and B) standardized to the UVB ($270 mJ/cm^2$) component is applied. Even with relatively mild sunburn a vast number of changes in skin physiology and structure are induced that could affect NP penetration. For example, within the first few hours prostaglandin synthesis can be observed[41,42,43]. Prostaglandins target the E-cadherin regulating receptors such that within hours E-cadherin levels are significantly decreased[40]. Expression of tight junction related proteins (ZO-1, claudin-1 and occludin) are also known to be perturbed following UVB exposure[44]. These proteins are important in considering NP penetration through UVR exposed skin, as they promote intercellular adhesions. Loosening of these adhesions allows for the corresponding cellular proliferative response to quickly replenish differentiating epidermal cells that form a thicken stratum corneum layer[45]. While this UVR repair process initiates, NP may encounter loosened intercellular adhesions causing an outside-in defect that could favor penetration. Alternatively, one can imagine that the accelerated keratinocyte proliferation and differentiation response enhances the net migration of cells to the skin surface which may help prevent NP translocation. Clearly, the competing processes of loosened intercellular junctions, oxidative damage and the hyperplasia response of the epidermis following exposure to a damaging UVR dose all provide potential mechanisms to impact the permeability of NP through skin. The *in vivo* model presented here comprises our initial effort to assess these effects. This model greatly advances the current state as it eliminates

the need for keeping *ex vivo* tissue viable during the experimental course and allows normal progression of the UVR inflammatory and hyperplasia responses and other skin barrier effects to be experimental variables.

Materials and Methods

Quantum Dots and Vehicle Preparation

To explore the effects of NP skin penetration using an *in vivo* model, we prepared QD in a vehicle appropriate for skin application and quantified its material properties. A key challenge in designing *in vivo* experiments is that it is not possible to have a large volume of application fluid or to protect the application area to keep fluid from evaporating, as the animal is still mobile and occlusion of the skin significantly affects barrier function[46]. In this work we chose to design an application vehicle containing 75% glycerol mixed with 25% carboxyl QD (Invitrogen ITK 565nm emission) stock solution (pH=9.0 borate buffer, 8μM QD). We chose glycerol as the diluent for several reasons. It is present in many commercial cosmetics; it is viscous, allowing it to be spread evenly on the backs of the mice without dripping off; it is of a similar pH to the surface of the skin (pH~5)[47], which will prevent any pH driven barrier effects, and it is hygroscopic preventing quick drying that would cause QD clumping and affect penetration. To ensure that glycerol did not negatively affect the stability of the QD solution we made particle size measurements using a Malvern Instruments Zetasizer Nano ZS (Malvern Instruments Ltd, Worcestershire, United Kingdom) without sonication 2 and 24 hours after solution formulation with room temperature storage.

QD Application to Mice

To examine the skin penetration of QD, we used 6-7 week old outbred SKH-1 wild-type mice (Charles Laboratory) weighing 25-30g. Mice were allowed access to water and standard mouse feed *ad libitum* and housed under constant humidity and temperature with 1 per cage and 12 hour light/dark cycles during QD experiments. Our experimental design used n=2 mice at each exposure condition (UVR-exposed and unexposed) and at each time point (8 hours and 24 hours after QD application). Prior to application of the QD glycerol solution each mouse was fitted with an Elizabethan collar (Braintree Scientific, Braintree, MA) to prevent removal and ingestion of applied QD. Each mouse was treated with 10μL of the prepared QD solution applied over a ~6 cm^2 area of their back. This provided a final QD dose of ~3 pmol/cm^2. The collars minimally affected mouse behavior, with the only effect being a slightly more subdued activity level. Mice were sacrificed at two time points (8 and 24 hrs) following QD application. All procedures were approved by the Institutional Laboratory Animal Care and Use Committee of the University of Rochester Medical Center.

UV Radiation Protocol

Half of the mice in this experimental design were treated with a single UVR dose. During UVR exposure mice were housed one per cage in a standard laboratory setting according to procedures detailed elsewhere[41]. Briefly, mice were exposed at a distance of 15 inches to UVA Sun 340 lamps, which emit across the UVA (320-400nm) and UVB spectra (290-320nm). The lamps were calibrated to UVB output using an IL1700 light meter (International Light) with a SED 240 probe (255-320nm detection). The total dose was

calculated using the measured value and length of exposure. For our experiments, the irradiated mice were exposed to an acute dose of 270 mJ/ cm^2 UVB. Within the 24 hr time frame of this experiment mice do not exhibit obvious signs of sun damage on their skin. Mice living longer (3-5 days post UVR exposure) do however develop a noticeable erythematous response on their backs[41]. The QD solution is applied to UVR treated mice immediately (within 1hr) according the procedure described above. The QD solution is also applied to the non-UVR treated mice (control) at the same time.

Skin Tissue Cryo-Processing

After sacrificing the mice, tissue was harvested using several techniques. A portion of the skin was snap frozen using liquid nitrogen and stored at -80°C. These samples were processed for analysis by mounting the skin in TEK OCT (Sakura FineTek USA Inc. Torrance, CA). Skin was sliced onto a microscope slide using a Microm HM 525 cryostat (Mikron Instruments, Inc. San Marcos, CA) at 10μm thickness, with the blade changed between slices and slicing from the dermis to epidermis. The blade precautions were taken to avoid accidental transfer of QD from the skin surface to epidermal and dermal layers when slicing. After slicing, all frozen sections were fixed in 5% formalin in PBS for 10 minutes. They were then stained lightly with Gill's Hematoxylin and mounted using Vectashield DAPI mounting media (Vector Laboratories, Inc. Bulingame, CA). To help highlight the stratum corneum, frozen sections fixed in 5% formalin were blocked using CAS-BLOCK (Invitrogen Corp. Carlsbad, CA) and incubated with rabbit anti-mouse Loricrin antibody (Covance, Berkeley, CA) for 90 minutes. After washing with PBS, a goat anti-rabbit Texas Red secondary antibody (Rockland Immunochemicals, Inc. Gilbertsville, PA) was then applied for 90 minutes to develop the color. Loricrin was chosen because it is a very late releasing protein in the stratum granulosum that is present in large quantities in the stratum corneum[48]. The slices were analyzed under fluorescence microscopy (Nikon Eclipse E800 with a Spot RTS camera) with a long-pass filter (355-365nm excitation and emission of 420nm and up) for collection and penetration trends. To help evaluate the effect of UVR exposure on QD skin penetration, we measured the thickness of the stratum corneum using Spot Advance software. For each mouse, two different slices were photographed in three locations at 40X magnification. Each was then measured five times, giving a total of n=60 for each treatment condition. A 3-way ANOVA test was performed using the MATLAB statistics toolbox with a confidence level of 99%. Data collection was randomized to ensure no bias was introduced by the experimenter.

Confocal Microscopy

To provide support for our fluorescent microscopy findings, further examination of the QD skin penetration profiles was performed using fluorescence confocal microscopy. Whole skin samples were mounted in a Mowiol 4-88 (Sigma 81381) mounting media containing glycerol before imaging using an upright DMRE Leica TCS SP Spectral Confocal microscope equipped with StereoInvestigator software (MBF Bioscience, Williston, VT) and excitation from a 488 nm argon laser. The tissue from each was imaged by differential interference microscopy (DIC) and with a narrow fluorescence window (555-585 nm) to image target QD emission (~565 nm) only. Acquisition of 0.5 μm confocal slices was taken

through the thickness of the skin samples (~25 μm) using the StereoInvestigator software. 3D stack reconstruction and image processing was performed using ImageJ software (NIH).

Transmission Electron Microscopy

Transmission electron microscopy (TEM) was used to examine ultrastructural details of QD nanoparticle skin penetration through the skin and their end locations at the cellular level. After 24 hour fixation in 2.5% glutaraldehyde, the whole skin samples were postfixed in osmium tetroxide and silver enhanced using a standard AURION R-GENT SE-EM reagent and protocol. The silver enhancement selectively deposited on the QD to allow them to be distinguished easily from the surrounding tissue. After silver enhancement of the QD, the skin samples were dehydrated using graded alcohol baths (25%, 50%, 75% and 100%) and then infiltrated with and embedded in Spurr epoxy resin with overnight polymerization at 70°C. After embedding, the samples were cut to 1-2 μm with a glass blade and finally sliced at 70nm with a diamond knife and placed on copper grids. The nanoparticle localization was evaluated using the Hitachi 5100 TEM apparatus with EDAX attachment to provide elemental analysis spectra of samples. To ensure silver enhancement only worked on QD, a negative control was processed from a mouse with glycerol only. After silver enhancement, dehydration, epoxy mounting, and slicing, measurements were performed on the negative control sample (no QD) using equivalent procedures as with QD exposed skin samples.

Results and Discussion

Application Vehicle Characterization

In designing our experiment, the first concern was formulation of an application vehicle and demonstration that QD size stability was unaffected. Glycerol was identified as a potential diluent. Particle size analysis, summarized in Fig. 1 (raw data Fig. S1), revealed that QD prepared in deionized (DI) water and in 75% glycerol remain monodispersed exhibiting a particle size of ~20 and ~33 nm, respectively. QD formulated in DI water and glycerol remain stable after storing the solution at room temperature for at least 24 hr. Zeta potential measurements in DI water suggest a weak negative surface charge of approximately -20 mV. Surface charge measurements in 75% glycerol could not be made due to instrumentation limitations resulting from high solution viscosity. However, zeta potential measurements made at lower glycerol levels (25% and 50%) suggest the QD retain their intrinsic negative surface charge as measured in DI water. The hygroscopic properties and pH matching of glycerol (pH~5.8) to the stratum corneum[47,49] (pH~5.5) combined with a stable particle size over the time period of interest (24hr) suggested glycerol as an ideal QD application vehicle for our *in vivo* experiments. This vehicle enabled application of a small volume of fluid that was easily spread over the application area and provided humectant properties, preventing rapid evaporation.

Validation of UVR Induced Skin Response

After processing skin tissue with the methods described, hematoxylin stained cryopreserved tissue sections were examined under bright field optical microscopy to validate evidence for the biological effects of exposure to UVR in our model system. It is known that UVR exposure to skin affects keratinocyte differentiation and cell division in the epidermis. This

UVR induced skin repair response causes a rapid increase in epidermal proliferation and differentiation events with a resultant thickening of the stratum corneum and hyperplasia of the epidermis that initiates within hours after UVR exposure and remains elevated for more than 3 days[43]. Validation of these responses in our model system after just 24 hr is important as epidermal remodeling may potentiate an outside-in barrier defect allowing for enhanced QD NP skin penetration. In this work we used stratum corneum (SC) thickening as a metric. Our results confirm the induction of the UVR repair response as stratum corneum thickening was clearly observable even after only 8 hours (Fig. 2). After 24 hours, the difference in stratum corneum thickness between the unexposed and UVR exposed samples was pronounced, increasing from ~9.7 μm to 18.9 μm, respectively. It is interesting to note that there is a statistically significant difference between the 8 hour UVR exposed and 24 hour UVR exposed samples, validating that the UVR induced keratinocyte proliferation and differentiation response had initiated. It is also important to note that ANOVA testing criteria at a 1% confidence level found no observable difference between the 8 hour and 24 hour non-UVR exposed samples. This is of note as it suggests that the applied QD mixture did not affect the stratum corneum thickness, and therefore can be thought to have a minimal effect on keratinocyte proliferation and differentiation. Histological studies (described below) found no evidence for immune infiltration in the non-UVR exposed samples, further suggesting a negligible effect of QD application to non-UVR exposed skin over the studied time course. In contrast to the SC, epidermal thickening was not as pronounced in the 24 hour time period (Fig. S2). This is consistent with expectation, as the UVR induced hyperkeratosis (stratum corneum thickening) response has been shown to increase more quickly than the hyperplasia response (epidermal thickening)[45,50]. Analysis of skin samples 4.5 days post UVR exposure (Fig. S3) confirm the progression of gross morphological changes in both the epidermis and stratum corneum. The ability to quantifiably measure physical evidence of the biological response to UVR exposure provides evidence of a UVR induced repair process that includes down regulation of E-cadherins[40] and alteration in the expression of tight junction proteins[44]. It is of interest to investigate how the competing effects of loosened cell junctions and accelerated cellular proliferation, differentiation, and migration toward the skin surface combine to impact NP penetration.

QD Penetration- Effect of UV

To examine QD penetration, the histological slices provided important insights. Results consistently found a similar trend of increased penetration for both treatment conditions (8 hours and 24 hours) with UVR. Most strikingly, under no circumstances is there evidence for massive QD penetration- even for UVR exposed mice 24 hours after QD application. Our data consistently find that QD preferentially collect in folds and defects in the stratum corneum (Fig. 3a, Fig. S4) as well as in hair follicles (Fig. 3b). The collection effect is seen even in the non-UVR exposed mice. Underneath the folds and defects, there are often fewer stratum corneum layers and a thinner epidermal layer, which could potentially increase long term risk of penetration at these sites. The collection of NP in folds, defects, and hair follicles is a well documented phenomenon[16,51] that is specific to NP in the size range used in our experiments, and may contribute to increased penetration over time and provide an opportunity for targeted drug delivery applications through the follicle[16,52,53].

To provide further evidence of this occurrence, we used whole tissue fluorescence confocal imaging. The confocal imaging provided us with a clear 3-D perspective on the collection phenomenon, as it showed a profile with QD collecting all the way into the lower portions of the hair shaft (Fig. 4). The confocal imaging also serves to highlight the much larger proportion of QD available in folds/defects and especially the hair follicle.

Despite the similarities in trends throughout the different time and UVR exposure conditions, there were some distinct differences between the samples in terms of penetration levels. To explore the differences in mouse skin penetration between the time points and UVR exposures, we first consider the cryo-preserved tissue sections. It is important to reiterate that none of the penetration observed was at a very high level, but we were able to observe increased penetration for the UVR as compared to the control at both the 8hr and 24hr time points (Fig. 5). The 8 hour UVR exposed samples showed a higher rate of penetration over the 8 hr control. This was seen in a variety of structures, but appears most commonly in areas that have a defect in the stratum corneum or by hair follicles (Fig. 5B). This trend is mirrored at the 24 hr time point as well. The difference between the 8hr UV and 24hr UV mice is not as marked. The deepest levels that showed evidence of QD was an additional point of interest. Presence into the stratum corneum could be observed throughout all skin samples (Fig. 3a). In a few isolated locations for the non-UV exposed mice, some of the outermost keratinocytes demonstrated QD presence in what appeared to be perinuclear locations (Fig. 3a,ii). However, the presence was far greater throughout the UV exposed mice, which showed additional QD presence much deeper in the tissue. Tissue levels as deep as the dermis were common, but still at low levels. Common trends and more detailed description of these instances will be shown in greater detail in future work which will seek a more detailed understanding of the relative importance of para- and trans-cellular transport mechanisms as well as to identify differences that may result from a change in application conditions, such as more severe UVR damage or application of QD at a longer time point after UVR exposure.

QD Penetration - Mechanistic Insight

To provide mechanistic insight into the penetration pathway taken by QD to breach the stratum corneum barrier, TEM with silver enhancement was used. The silver enhancement procedure increases QD particle size to ~35-45 nm (Fig. S5) and allows clear imaging of them against the tissue background. EDAX was used to determine the elemental composition of the spots believed to be silver enhanced QD, and found a strong presence of silver in all cases of spots believed to be NP (Fig. 7). TEM provided convincing evidence that the QD were getting through the stratum corneum through the intercellular lipid lamellae along the edges of the differentiated corneocytes (Fig. 6a,b). To confirm that silver enhancement was selective for the QD, a control mouse (24 hr UVR but no QD, 75% glycerol only) was examined (Fig. 6d) and spectra taken of suspicious debris (Fig. S6). No presence of silver could be found in any of the suspicious dark spots on non-QD control samples. It is our observation from analysis of a number of the experimental tissue slices that silver enhanced QD are more frequently seen in viable epidermal layers such as the stratum granulosum (Fig. 6c) using TEM compared to cryohistology analysis. There were

also a number of QD present deeper in the dermis that were taken up by various cell types and dermal structures (details to be published elsewhere).

Conclusion

These studies demonstrate the importance of skin condition to effect the penetration of QD nanoparticles (~30 nm dia) in the *in vivo* SKH-1 mouse model. We have shown that QD work their way between the corneocytes of the stratum corneum and penetrate deep in the epidermis and dermis of an *in vivo* model with UVR penetration exacerbation. This is an important advancement as it suggests that UVR induces an outside-in barrier defect likely due to a loss of epidermal calcium gradient and resultant stratum corneum lipid disruption[7,54], and through loosening of cell-cell junctions that down regulate following an acute UVR exposure. The accelerated epidermal proliferation and differentiation UVR skin repair response is insufficient to prevent QD from breeching the skin barrier. It is important to note that the penetration of QD did not attain the drastic levels seen in some *ex vivo* nanoparticle tissue studies[12] even with mechanical flexing associated with normal animal motion[14]. The collection of NP in folds, defects, and hair follicles provides a possible mechanism for transport when taken together with the barrier function disruption and stratum corneum intercellular weakening effect of UVR[40]. We believe that the QD penetration is strongly dependent on the condition of the skin and the characteristics of the QD (size and surface chemistry). This is an important discovery for nanoparticle safety concerns as consumers often apply sunscreens containing metal oxide nanoparticles of similar size and raw material properties to UV-exposed skin. The minimal QD penetration observed in our study on barrier intact (non-UVR exposed) skin supports the preponderance of current literature suggesting TiO_2 and ZnO NP used in commercial sunscreens exhibits limited penetration in layers below the lower SC[8,55]. The increased QD penetration seen with UVR damage raises concern, but this result does not directly address the issue of metal oxide NP penetration through UVR damaged skin. A wide variety of surface coatings on TiO_2 and ZnO NP are used in formulating commercial sunscreens to make them waterproof and to improve their application characteristics. These coatings may alter their skin penetration characteristics. Future studies are planned to develop our ability to quantify the amount of QD penetration. We will apply our techniques to a variety of QD surface chemistries to provide an essential understanding of surface coating dependent penetration mechanisms at the cellular level. Additionally, future *in vivo* studies using custom imaging modalities and commercial sunscreen formulations are planned to generate the necessary insight to assess human health risks from applying NP sunscreens to UV-exposed skin.

Supplementary Material

Refer to Web version on PubMed Central for supplementary material.

Acknowledgments

References

1. Akermann ME, Chan WCW, Laakkonen P, Bhatia SN, Ruoslahti E. PNAS. 2002; 99:12617. [PubMed: 12235356]

2. Serpone N, Emeline AV. Res Chem Intermed. 2005; 31:391.

3. Chen X, Schluesener HJ. Toxicology Letters. 2008; 176:1. [PubMed: 18022772]

4. Hardman R. Environmental Health. 2006; 114(2):165.

5. Oberdörster G, Oberdörster E, Oberdörster J. Environmental Health Perspectives. 2005; 113(71): 823–839. [PubMed: 16002369]

6. Blue Lizard Sunscreens. Crown Laboratories, Inc.; Johnson City, TN:

7. Jiang SJ, Chen JY, Lu ZF, Yao J, Che DF, Zhou XJ. J Dermatol Sci. 2006; 44:29. [PubMed: 16842978]

8. Gamer AO, Leibold E, van Ravanzwaay B. Toxicol In Vitro. 2006; 20:301. [PubMed: 16182508]

9. Lademann J, Weigmann HJ, Rickmeyer C, Barthlemes H, Schaefer H, Mueller G, Sterry W. Skin Pharmacol Appl Skin Physiol. 1999; 12:247. [PubMed: 10461093]

10. Pflücker F, Wendel V, Hohenberg H, Gärtner E, Will T, Pfeiffer S, Wepf R, Gers-Barlag H. Skin Pharm Appl Skin Physiol. 2001; 14:92.

11. Schulz J, Hohenberg H, Pflücker F, Gartner E, Will T, Pfeiffer S, Wepf R, Wendel V, Gers-Barlag H, Wittern KP. Adv Drug Deliv Rev. 2002; 54(Suppl 1):S157. [PubMed: 12460721]

12. Ryman-Rasmussen JP, Riviere JE, Monteiro-Riviere NA. Toxicol Sci. 2006; 91:159. [PubMed: 16443688]

13. Zhang LW, Yu WW, Colvin VL, Monteiro-Riviere NA. Toxicol and Appl Pharmacol. 2008; 228:200. [PubMed: 18261754]

14. Rouse JG, Yang J, Ryman-Rasmussen JP, Barron AR, Monteiro-Riviere NA. Nano Lett. 2007; 7:155. [PubMed: 17212456]

15. Baroli B, Ennas MG, Loffredo F, Isola M, Pinna R, Lopez-Quintela MA. J Dermatol Sci. 2007; 127:1701–1712.

16. Toll R, Jacobi U, Richter H, Lademann J, Schaefer H, Blume-Peytavi U. J Dermatol Sci. 2004; 123:168.

17. Tinkle SS, Antonini JM, Rich BA, Roberts JR, Salmen R, DePree K, Adkins EJ. Environ Health Perspect. 2003; 111:1202. [PubMed: 12842774]

18. Chang E, Thekkek N, Yu WW, Colvin VL, Drezek R. Small. 2006; 2:1412. [PubMed: 17192996]

19. Akerman ME, Chan WCW, Laakkonen P, Bhatia SN, Ruoslahti E. Proc Natl Acad Sci. 2002; 99:12617. [PubMed: 12235356]

20. Maysinger D, Lovric J, Eisenberg A, Savic R. Euro J Pharm Biopharm. 2007; 65:270.

21. Lovric J, Bazzi HS, Cuie Y, Fortin GRA, Winnik FM, Maysinger D. J Mol Med. 2005; 83:377. [PubMed: 15688234]

22. Long TC, Saleh N, Tilton RD, Lowry GV, Veronesi B. Environ Sci Technol. 2006; 40:4346. [PubMed: 16903269]

23. Kang JL, Moon C, Lee HS, Lee HW, Park EM, Kim HS, Castranova V. J Toxicol Environ Health A. 2008; 71:478. [PubMed: 18338282]

24. Wamer WG, Yin JJ, Wei RR. Free Radical Biol. 1997; 23:66.

25. Ryman-Rasmussen JP, Riviere JE, Monteiro-Riviere NA. J Invest Dermatol. 2007; 127:143. [PubMed: 16902417]

26. Hussain SM, Hess KL, Gearhart JM, Geiss KT, Schlager JJ. Toxicol In Vitro. 2005; 19:975. [PubMed: 16125895]

27. Peters K, Unger RE, Kirkpatrick CJ, Gatti AM, Monari E. J Mater Sci Mater Med. 2004; 15:321. [PubMed: 15332593]

28. Gurr JR, Wang ASS, Chen CH, Jan KY. Toxicology. 2005; 213:66. [PubMed: 15970370]

29. Zhang AP, Sun YP. World J Gastroenterol. 2004; 10:3191. [PubMed: 15457572]

30. Nakagawa Y, Wakuri S, Sakamoto K, Tanaka N. Mutation Research. 1997; 394:125. [PubMed: 9434851]

31. Linnainmaa K, Kiveipensa P, Vainio H. Toxicol In Vitro. 1997; 11:329. [PubMed: 20654319]

32. Konaka R, Kasahara E, Dunlap WC, Yamamoto Y, Chien KC, Inoue M. Free Radic Biol Med. 1999; 27:294. [PubMed: 10468201]

33. Reeves JF, Davies SJ, Dodd NJF, Jha AN. Mutation Research. 2008; 640:113. [PubMed: 18258270]

34. Sayes CM, Wahi R, Kurian PA, Liu Y, West JL, Ausman KD, Warheit DB, Colvin VL. Toxicol Sci. 2006; 92:174. [PubMed: 16613837]

35. Serpone N, Emeline AV. Res Chem Intermed. 2005; 31:391.

36. Dabbousi BO, Rodriguez-Viejo J, Mikulec FV, Mattoussi H, Ober R, Jensen KF, Bawendi MG. J Phys Chem B. 1997; 101:9463.

37. Yu WW, Chang E, Drezek R, Colvin VL. Biochem and Biophys Res Commun. 2006; 348:781. [PubMed: 16904647]

38. Kligman LH, Kligman AM. J Natl Cancer Inst. 1981; 67:1289. [PubMed: 6947111]

39. Pentland AP, Scott G, VanBuskirk J, Tanck C, LaRossa G, Brouxhon S. Cancer Res. 2004; 64:5587. [PubMed: 15313895]

40. Brouxhon S, Kyrkanides S, O'Banion MK, Johnson R, Pearce DA, Centola GM, Miller JH, McGrath KH, Erdle B, Scott G, Schneider S, VanBuskirk J, Pentland AP. Cancer Res. 2007; 67:7654. [PubMed: 17699770]

41. Brouxhon S, Konger RL, VanBuskirk J, Sheu TJ, Ryan J, Erdle B, Almudevar A, Breyer RM, Scott G, Pentland AP. J Invest Dermatol. 2007; 127:439. [PubMed: 16977324]

42. Pentland AP, Mahoney M, Jacobs SC, Holtzman MJ. J Clin Invest. 1990; 86:566. [PubMed: 1696589]

43. Tripp CS, Blomme EAG, Chinn KS, Hardy MM, LaCelle P, Pentland AP. J Invest Dermatol. 2003; 121:853. [PubMed: 14632205]

44. Yamamoto T, Kurasawa M, Hattori T, Maeda T, Nakano H, Sasaki H. Arch Dermatol Res. 2008; 300:61. [PubMed: 18064478]

45. Haratake A, Uchida Y, Schmuth M, Tanno O, Yasuda R, Epstein JH, Elias PM, Holleran WM. J Invest Dermatol. 1997; 108:769. [PubMed: 9129231]

46. Wood LC, Elias PM, Calhoun C, Tsai JC, Grunfeld C, Feingold KR. J Invest Dermatol. 1996; 106:397. [PubMed: 8648167]

47. Wagner H, Kostka KH, Lehr CM, Schaefer UF. Euro J Pharma Biopharma. 2003; 55:57.

48. Mehrel M, Hohl D, Rothnagel JA, Longley MA, Bundman D, Cheng C, Lichti U, Bisher ME, Steven AC, Steinert PM, Yuspa SH, Roop DR. Cell. 1990; 61:1103. [PubMed: 2190691]

49. Ehlers C, Ivens UI, Moller ML, Senderovitz T, Serup J. Skin Res Technol. 2001; 7:90. [PubMed: 11393210]

50. Akitomo Y, Akamatsu H, Okano Y, Masaki H, Horio T. J Dermatol Sci. 2003; 31:151. [PubMed: 12670726]

51. Alvarez-Roman R, Naik A, Kalia Y, Guy RH, Fessi H. J Control Release. 2004; 99:53. [PubMed: 15342180]

52. Vogt A, Combadiere B, Hadam S, Stieler K, Lademann J, Schaefer H, Autran B, Sterry W, Blume-Peytavi U. J Invest Dermatol. 2006; 126:1316. [PubMed: 16614727]

53. Vogt A, Mandt N, Lademann J, Schaefer H, Blume-Peytavi U. J Invest Dermatol Symp Proc. 2005; 10:252.

54. Jiang SJ, Chu AW, Lu ZF, Pan MH, Che DF, Zhou XJ. Exp Dermatol. 2007; 16:985. [PubMed: 18031457]

55. Cross SE, Innes B, Roberts MS, Tsuzuki T, Robertson TA, McCormick P. Skin Pharmacol Physiol. 2007; 20:148. [PubMed: 17230054]
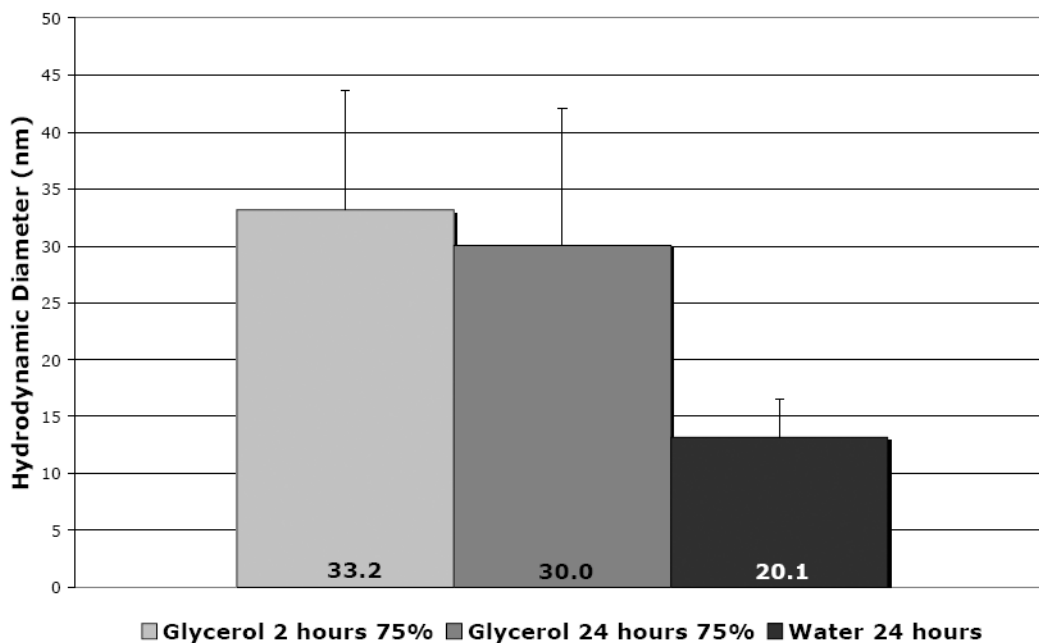
Figure 1.
The relative size of quantum dot nanoparticles as measured using a Malvern Zetasizer. All measurements are the average of 6 measurements per sample. The 75% glycerol QD show a larger size, but the average remains similar over the time course of our experiment (24 hours), with a small increase in the distribution of the peak width (Fig. S1). The size in 75% glycerol solution compares well with that in deionized (DI) water.
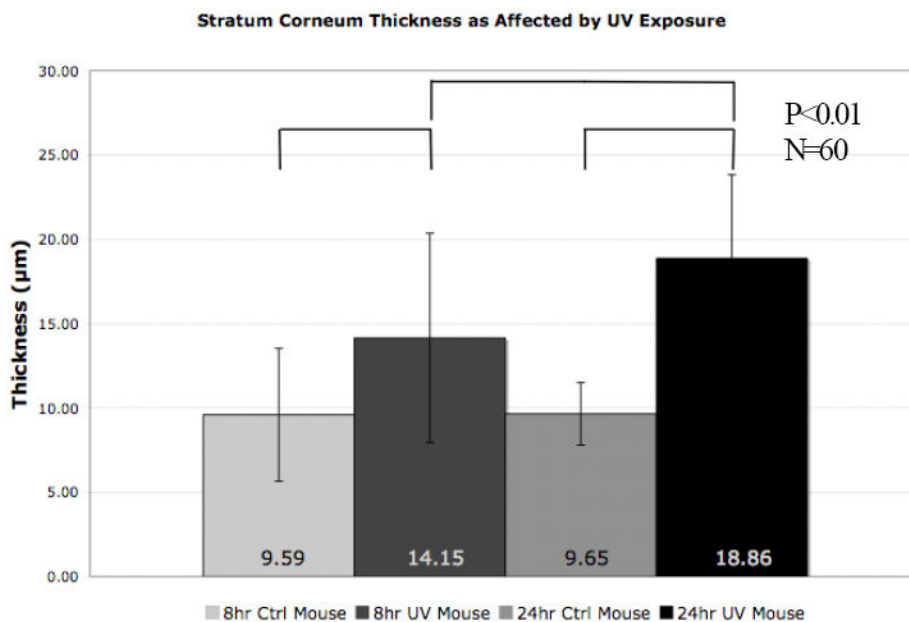
Stratum Corneum Thickness as Affected by UV Exposure

Figure 2.
The stratum corneum shows thickening as the keratinocytes quickly differentiate into mature corneocytes in response to UVR light exposure. The differentiation response- as measured by stratum corneum thickness- increases with time after UVR exposure. The unexposed mice do not show a thickening response despite presence of the QD borate buffer/glycerol solution. Each of the UVR exposed conditions are at a 99% confidence level of difference from each other and the controls.
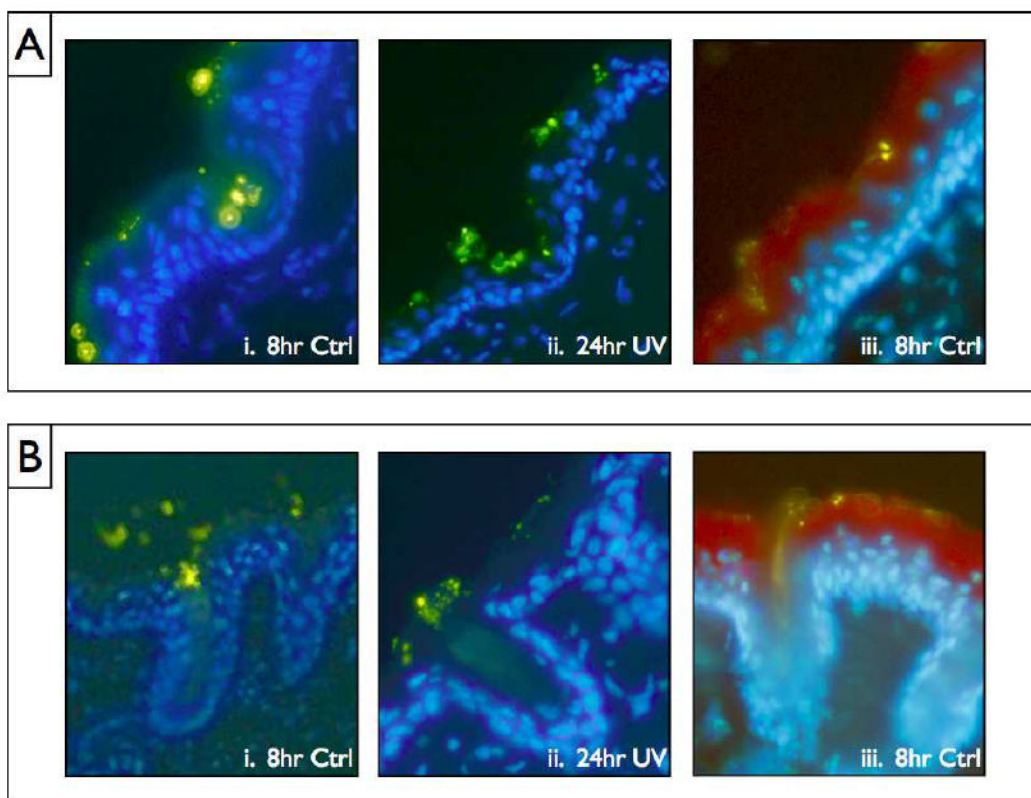
Figure 3.
(A) The common collection pattern of QD in skin defects and folds observed throughout the samples. The weaknesses in the stratum corneum that are present in many of these cases may contribute to increased stratum corneum penetration possibility. (B) Three examples of the collection pattern commonly occurring in the mouse hair follicles. i. and ii. Are stained with DAPI blue and iii. Is stained with a combination of DAPI and Texas Red Loricrin antibody, a protein found in high abundance in the stratum corneum. The Greenish/yellow spots are the QD.
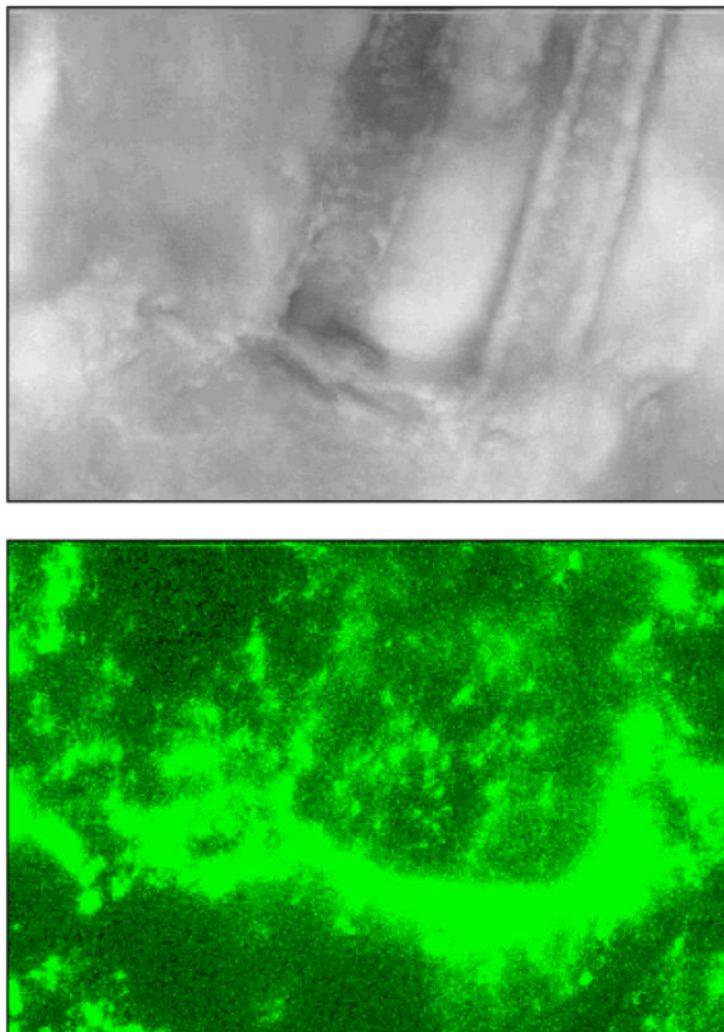
Figure 4.
A confocal image taken at 40x magnification. The top image is the differential interference contrast (DIC) image that shows twin hairs going under the surface of the skin. The bottom image is the same field of view with a 555-585nm fluorescence window to illuminate the QD. The side and bottom profile the 3-dimensional stack of images (fluorescence into the skin), giving a clear view of the depth and hair follicle location of a large quantity of QD.
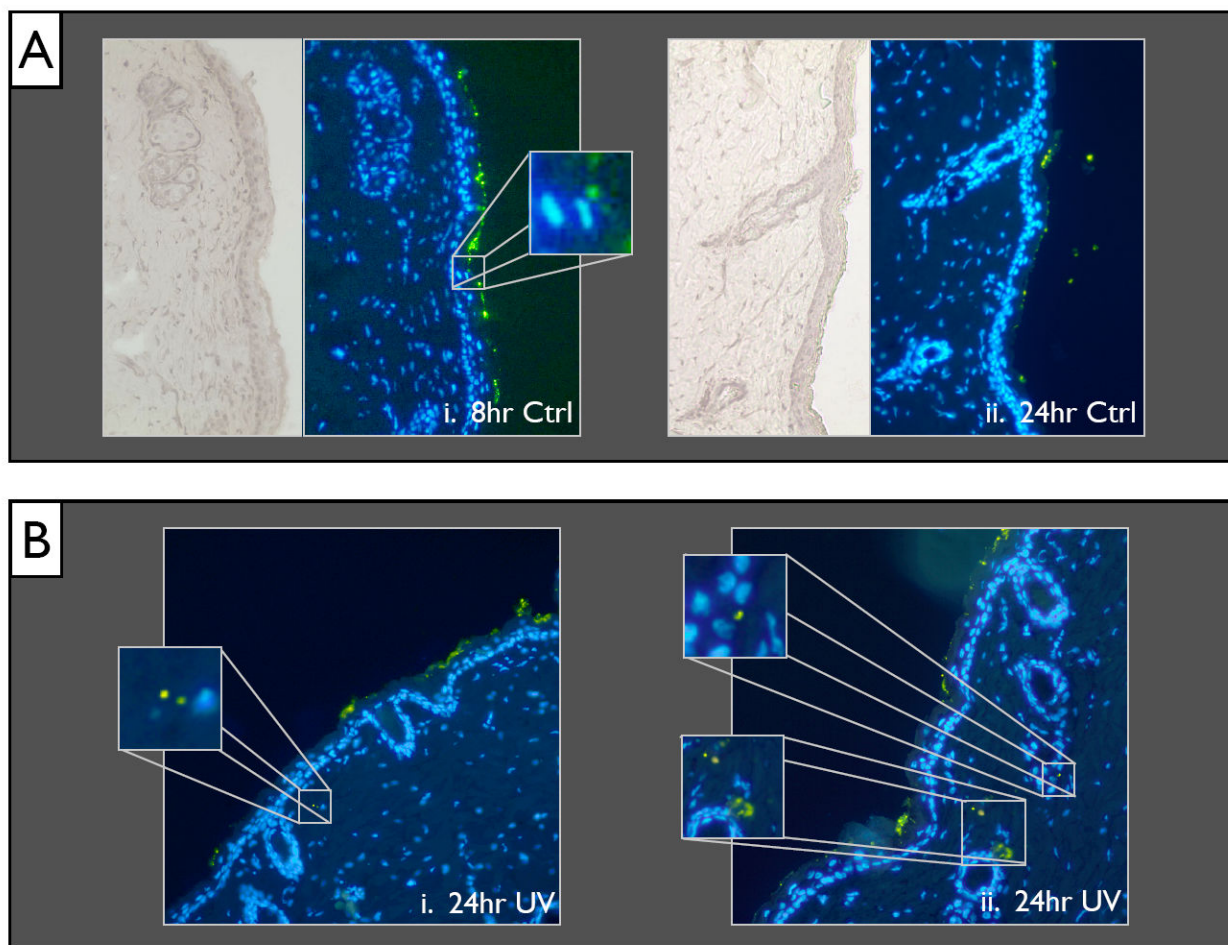
Figure 5.
(A) An overview (20x magnification) of the 8hr Ctrl (i) and 24hr Ctrl (ii). Minimal presence of QD can be seen even in the lower stratum corneum layers. (B) Example slices of the 24hr UVR exposed mouse skin with high penetration areas in the dermis highlighted by magnified insets.
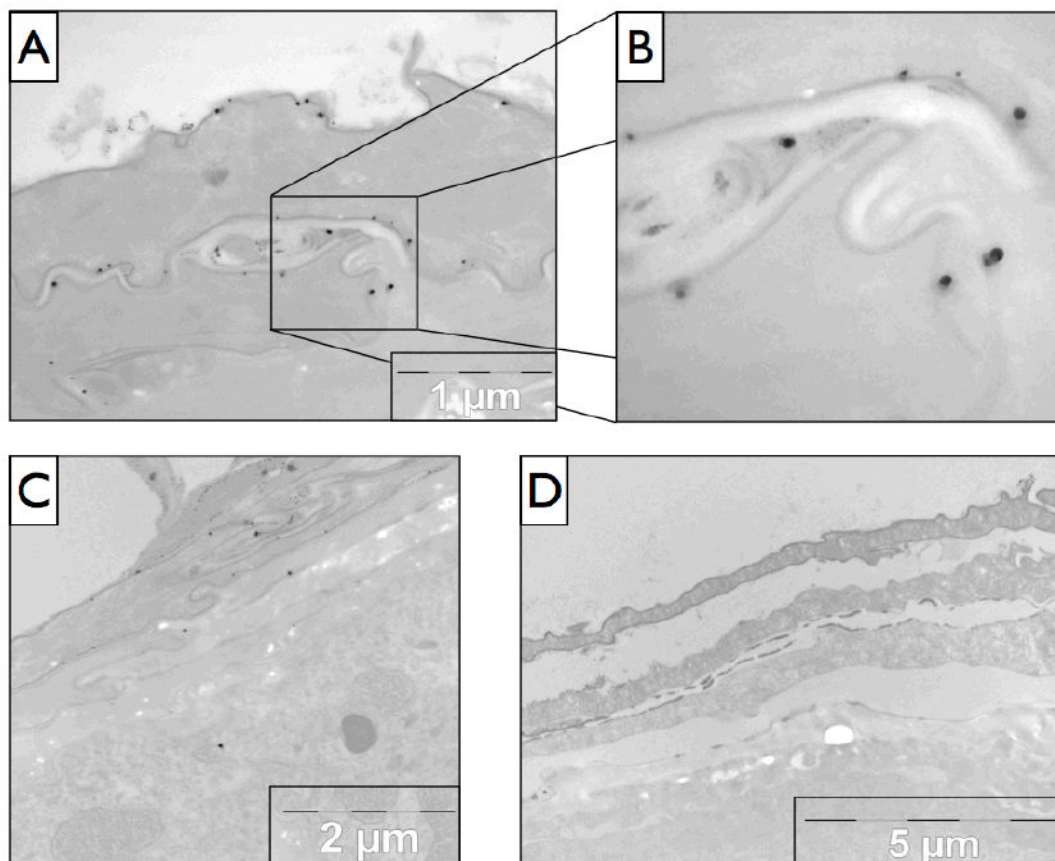
Figure 6.
TEM imaging of 24hr UVR exposed mouse skin sections. (A) The penetration pathway through the skin can be clearly seen, and is shown in more detail in (B) with the large dark spots being the NP. (C) Another section of skin demonstrating the penetration pathway and with an example silver enhanced QD present in the epidermal layer. (D) The negative control (no QD, glycerol only) of silver enhanced mouse skin 24 hr UVR exposure.
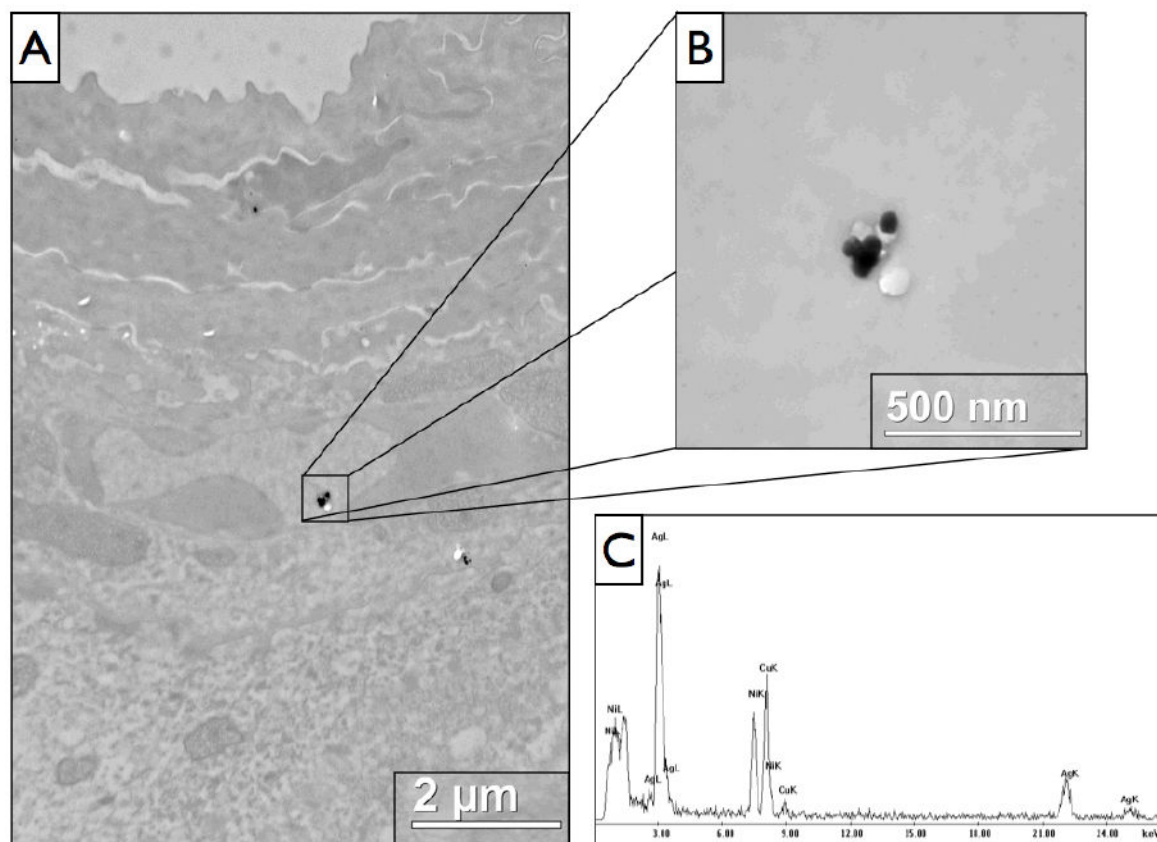
Figure 7.
TEM analysis of 24 hour UVR exposed mouse skin with EDAX evaluation of elemental composition. The quantum dot components are unable to be detected, but with selective silver enhancement, silver peaks are clearly visible in the spectra. **(A)** A lower magnification view showing the presence of a couple silver enhanced QD clusters in the stratum granulosum. **(B)** A higher magnification view of the larger cluster of silver enhanced QD. **(C)** The EDAX spectrum for the cluster shown in (B), demonstrating a strong presence of silver, with additional presence of copper and nickel that are elements present in the TEM grid used.